## Structural kinetics of myosin by transient time-resolved FRET

Yuri E. Nesmelov<sup>a,1,2</sup>, Roman V. Agafonov<sup>a</sup>, Igor V. Negrashov<sup>a</sup>, Sarah E. Blakely<sup>a</sup>, Margaret A. Titus<sup>b</sup>, and David D. Thomas<sup>a,1</sup>

<sup>a</sup>Department of Biochemistry, Molecular Biology and Biophysics, and <sup>b</sup>Department of Genetics, Cell Biology and Development, University of Minnesota Medical School, Minneapolis, MN 55455

Edited by James A. Spudich, Stanford University, Stanford, CA, and approved December 17, 2010 (received for review August 18, 2010)

For many proteins, especially for molecular motors and other enzymes, the functional mechanisms remain unsolved due to a gap between static structural data and kinetics. We have filled this gap by detecting structure and kinetics simultaneously. This structural kinetics experiment is made possible by a new technique, (TR)<sup>2</sup>FRET (transient time-resolved FRET), which resolves protein structural states on the submillisecond timescale during the transient phase of a biochemical reaction. (TR)<sup>2</sup>FRET is accomplished with a fluorescence instrument that uses a pulsed laser and direct waveform recording to acquire an accurate subnanosecond timeresolved fluorescence decay every 0.1 ms after stopped flow. To apply this method to myosin, we labeled the force-generating region site specifically with two probes, mixed rapidly with ATP to initiate the recovery stroke, and measured the interprobe distance by (TR)<sup>2</sup>FRET with high resolution in both space and time. We found that the relay helix bends during the recovery stroke, most of which occurs before ATP is hydrolyzed, and two structural states (relay helix straight and bent) are resolved in each nucleotide-bound biochemical state. Thus the structural transition of the force-generating region of myosin is only loosely coupled to the ATPase reaction, with conformational selection driving the motor mechanism.

disorder-to-order transition | myosin II | dictyostelium

**S** tructural dynamics lies at the heart of protein function. Transitions among distinct structural states, each characterized by both structural order and internal dynamic disorder, are typically required for the function of a protein, especially an enzyme. To describe the mechanism of a protein's function is to describe its *structural kinetics*, i.e., the coupling of protein structural transitions to biochemical kinetics, as defined by changes in bound ligand (1–3). However, for most proteins there remains mechanistic ambiguity due to a gap between structural data, determined primarily from static protein crystals, and kinetics, measured during the transient phase of the biochemical reaction. In the present study, we have closed this gap by measuring structure and kinetics simultaneously, using myosin as a powerful example.

In a molecular motor, ATP binding and hydrolysis initiate protein structural changes that lead to force generation, and characterization of motor protein structural kinetics is essential to understand the protein in action. Myosin is a molecular motor responsible for actin-dependent force generation and movement in muscle and nonmuscle cells; it works cyclically, producing mechanical work on actin using energy from ATP hydrolysis (recently reviewed in refs. 4 and 5). Transient kinetics in myosin has been typically monitored by tryptophan fluorescence (6, 7), but that signal provides no direct structural information. FRET does provide structural information, in the form of interprobe distance, and transient FRET experiments have provided a glimpse of structural kinetics in muscle and other proteins (8–10). However, previous transient FRET measurements have been limited to the monitoring of a single signal with continuous excitation and detection, whereas only nanosecond time-resolved FRET (TR-FRET), in response to pulsed excitation, can resolve multiple distances and quantitate disorder (11, 12). Therefore, we have developed a spectroscopic technique, transient time-resolved FRET ((TR)<sup>2</sup>FRET), in which a complete and accurate time-resolved fluorescence decay is recorded every 0.1 ms after stopped flow, 10<sup>5</sup> times faster than previously achieved (13). This method unambiguously resolves the kinetics of protein structural states (conformations) on the millisecond timescale. This approach is versatile and can be applied to a wide range of biological systems, revealing another dimension of insight into structural dynamics. In the present study, we have used it to resolve structural transitions within the force-generating region of myosin following the addition of ATP.

In the current working model for myosin's mechanism, the myosin head undergoes major structural changes twice during the ATPase cycle, producing the power stroke and the recovery stroke. Although numerous structures of myosin have been captured by X-ray crystallography (4), to a good approximation there are two principal classes of nucleotide-bound conformations that show significant differences in the overall shape of the head and in the force-generating region (14). These two structural states are designated  $M^*$  (green) and  $M^{**}$  (red) in Fig. 1. The recovery stroke is the transition from  $M^*$  to  $M^{**}$ , in which the entire head bends (Fig. 1A) and the relay helix undergoes a remarkably similar bend (Fig. 1B). Based on nucleotide analogs used to produce the crystal structures, and on Trp fluorescence changes observed in solution, a minimal kinetic mechanism is shown in Scheme 1, which suggests that there is a tight coupling between the biochemical state (defined by the bound nucleotide) and the structural state of myosin.

However, there is growing evidence that the coupling between biochemical and structural states in myosin is not tight (reviewed in ref. 4). Two different crystal structures of the myosin head can be trapped with a single nucleotide analog (14–16). Change in the intrinsic fluorescence of a myosin-nucleotide analog complex upon pressure and temperature jumps suggests a transition between two structural states of myosin (17). Spectroscopic data on myosin with probes at the active site (18, 19), in the forcegenerating region (11, 20, 21), or in the actin-binding cleft (22) show evidence for two resolved structural states (conformations) in the presence of a single biochemical state (bound ligand). TR-FRET has provided a clear structural picture of this phenomenon: With a single nucleotide analog bound to myosin, two distinct structural states ( $M^*$  straight and  $M^{**}$  bent) were resolved for the entire head (23) (Fig. 1A) or for the relay helix in the force-generating region (11) (Fig. 1B). All these data suggest

Author contributions: Y.E.N., R.V.A., and D.D.T. designed research; Y.E.N. and R.V.A. performed research; I.V.N., S.E.B., and M.A.T. contributed new reagents/analytic tools; Y.E.N., R.V.A., and I.V.N. analyzed data; and Y.E.N., R.V.A., and D.D.T. wrote the paper.

The authors declare no conflict of interest.

This article is a PNAS Direct Submission.

<sup>&</sup>lt;sup>1</sup>To whom correspondence may be addressed. Email: yuri.nesmelov@uncc.edu or ddt@umn.edu.

<sup>&</sup>lt;sup>2</sup>Present address: Department of Physics and Optical Science, University of North Carolina, Charlotte, NC 28223.

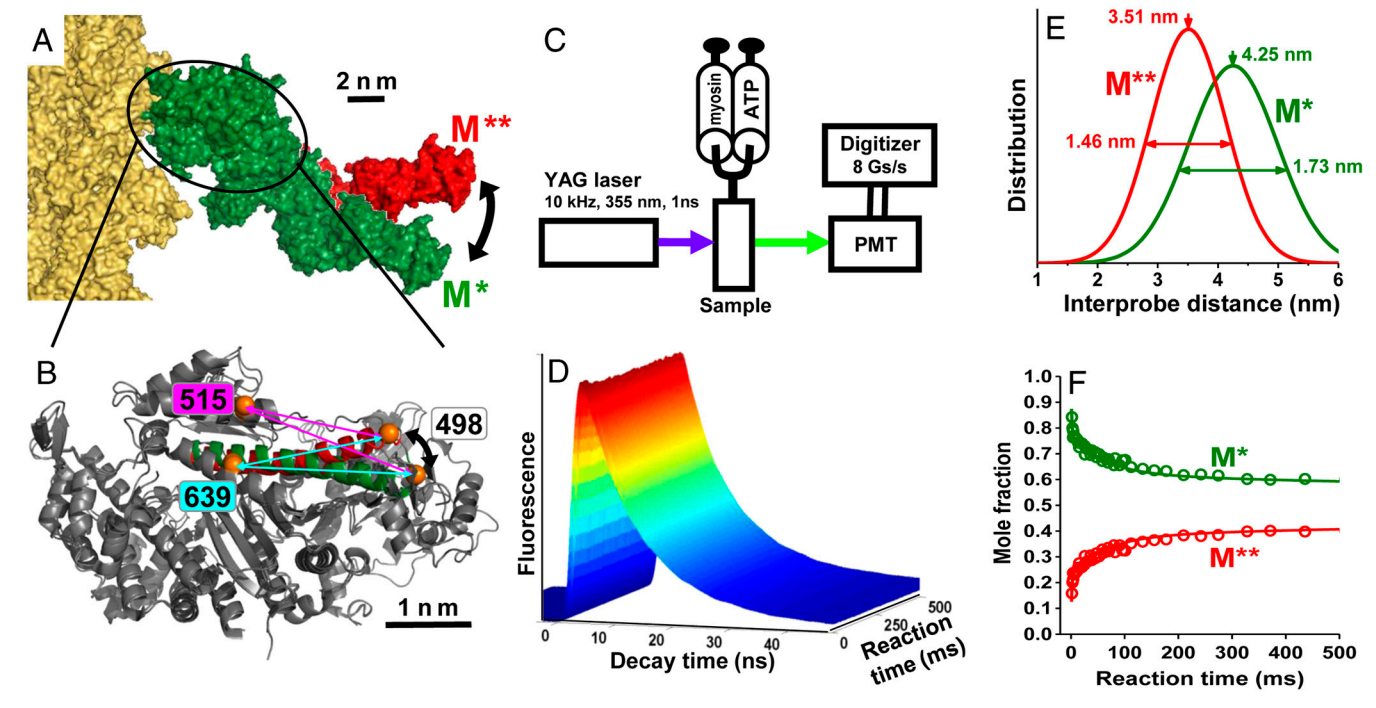


Fig. 1. Myosin structural change during the recovery stroke. (A) Myosin head S1 bound to actin (yellow) in the pre- (M\*, S1 green) and postrecovery (M\*\*, S1 red) states (4). (B) Myosin motor domain, overlay of crystal structures 1FMV (M\*, relay helix green) and 1VOM (M\*\*, relay helix red), showing proposed bending of the relay helix. Orange: engineered labeling sites, showing predicted shortening of distance between 639 and 498 (cyan arrows) and between 515 and 498 (magenta arrows) during the recovery stroke. (C) (TR)²FRET instrument. A stopped-flow apparatus (SFM-20, Bio-Logic) was attached to the TR-FRET fluorometer (11, 13). Myosin (labeled with FRET pair) and ATP solutions were loaded into syringes. A complete donor fluorescence waveform was acquired after every laser pulse (10,000 per second). (D) Data set from 498/639 pair at 20 °C, with 0.125-ns resolution in the fluorescence decay time (after laser pulse) and 0.1-ms resolution in the biochemical reaction time (after mixing of myosin and ATP). Global analysis, based on Scheme 2, gives simultaneously (E) the Gaussian interprobe distance distributions of each of the two structural states, and (F) biphasic kinetics of the structural transition. Forty-three log-distributed points are shown from each experimental trace. The best fit of Scheme 2 to the data is shown as solid curves. YAG, yttrium aluminum garnet.

the simultaneous presence of two distinct structural states of myosin,  $M^*$  and  $M^{**}$ , in one biochemical state, with the ATP hydrolysis step changing only the relative populations (mole fractions  $X^*$  and  $X^{**}$ ) of  $M^*$  and  $M^{**}$ . However, the assignment of these trapped nucleotide analog states to specific biochemical intermediates in the kinetic cycle is uncertain. Analysis of myosin's intrinsic fluorescence kinetics does suggest a branched mechanism of myosin-nucleotide interaction with two structurally different intermediates (5, 6, 17, 24), but this method does not have the structural resolution of TR-FRET. In order to obtain simultaneous structural and kinetic resolution, the present study uses (TR)<sup>2</sup>FRET (performing a complete TR-FRET experiment every 0.1 ms) to determine directly the structural kinetics within the myosin force-generating region during the myosin-ATP interaction and the recovery stroke (steps 1 and 2, Scheme 1 and Fig. 1A).

## **Results**

Relay Helix Structural Transitions Induced by the Myosin-ATP Interaction, Resolved in Real Time. We engineered two double-cysteine (Cys) mutants in a Cys-lite myosin construct, which had all reactive native cysteines removed (23). In each mutant, one labeling

$$\mathsf{M} \overset{k_1}{\rightleftharpoons} \mathsf{M}^\star.\mathsf{T} \overset{k_2}{\rightleftharpoons} \mathsf{M}^{\star\star}.\mathsf{D}.\mathsf{P} \overset{k_3}{\rightleftharpoons} \mathsf{M}^\star.\mathsf{D}.\mathsf{P} \overset{k_4}{\rightleftharpoons} \mathsf{M} \\ \overset{k_1}{k_4}$$

**Scheme 1.** Minimal kinetic ATPase mechanism for myosin, assuming rigid coupling of biochemical and structural states. *M*, myosin; *T*, ATP; *D*, ADP; and *P*, inorganic phosphate. *M*\* indicates a structural state with bound nucleotide in which both myosin head and relay helix are straight. *M*\*\* indicates a structural state with bound nucleotide in which both myosin head and relay helix are bent.

site is located at the C terminus of the relay helix (K498C) and another within the stable helices on the lower 50 kDa domain (D515C or A639C) (Fig. 1B). We labeled these cysteine residues with a donor–acceptor optical pair [(5-({2-[(iodoacetyl)amino] ethyl}amino)naphthalene-1-sulfonic acid) (IAEDANS), (4-((4-(dimethylamino)phenyl)azo)benzoic acid) (DABCYL)] (11). At equilibrium, with nucleotide analogs bound, the interprobe distance distribution was determined with both pulsed electron paramagnetic resonance and time-resolved FRET, with the resulting distances in good agreement with those measured from crystal structures, but both  $M^*$  (relay helix straight) and  $M^{**}$  (bent) structures were observed simultaneously (11).

To resolve transitions between myosin structural states with millisecond kinetic resolution during the recovery stroke, we designed and constructed the  $(TR)^2FRET$  fluorometer (Fig. 1C). This instrument is based on our recently reported high-performance time-resolved fluorescence (HPTRF) instrument, which improves the throughput for time-resolved fluorescence by a factor of 10<sup>5</sup> (13). Solutions of 5-mM ATP and 10-30-µM donoracceptor labeled myosin (syringe concentrations) were mixed in the fluorometer, and the complete time-resolved donor fluorescence decay was acquired after each laser pulse (10,000 times per second) immediately after myosin-ATP mixing (dead time 1.4 ms). The result is a two-dimensional dataset, resolved on both the nanosecond fluorescence decay timescale (0.125 ns per point) and the millisecond biochemical reaction timescale (0.1 ms per point) (Fig. 1D). At each time point in the millisecond-resolved transient, (TR)<sup>2</sup>FRET resolved distinct structural states of myosin, with essentially the same high resolution and precision as in previous equilibrium TR-FRET experiments (11). In TR-FRET, the decay rate of donor fluorescence increases with the inverse sixth power of the donor-acceptor distance R (Eq. 2). We fitted donor fluorescence decays globally as the sum of exponentials

(Eqs. 1–4), assuming two structural states, pre- and postrecovery  $(M^* \text{ and } M^{**})$ , corresponding to two interprobe distances,  $R^*$  and  $R^{**}$ , each with a distinct Gaussian distance distribution (Eq. 3 and Fig. 1E). The best fit to the data required two structural states; i.e., two states gave a better fit than one, but three states did not improve the fit. An excellent fit was obtained by assuming that these myosin structural states do not change during the course of the myosin-ATP interaction, but their populations ( $X^*$  and  $X^{**}$ ) do. After myosin-ATP mixing, the mole fraction  $X^{**}$  of myosin in the  $M^{**}$  structural state increases, as  $X^*$  decreases (Fig. 1F). By inspection of Fig. 1F, this recovery stroke is clearly biphasic, with one time constant of several milliseconds and the other at least 10 times slower. Kinetic traces for  $X^*$  and  $X^{**}$  populations were fitted by a system of differential equations (Eq. 5), corresponding to Scheme 2, assuming that the transition from the postrecovery stroke  $M^{**}.D.P$  state  $(k_4)$  is the rate-limiting step of the reaction (25).

The resulting rate constants are shown in Table 1. The first step in Scheme 2, ATP binding, is very fast, practically irreversible, and temperature independent ( $k_1$  and  $k_{-1}$ , Table 1). The recovery stroke  $(M^*.T \to M^{**}.T$ , characterized by  $k_2$  and  $k_{-2}$ ) and the hydrolysis step  $(M^{**}.T \to M^{**}.D.P$ , characterized by  $k_3$  and  $k_{-3}$ ) are temperature dependent. The recovery stroke, marked by the bending of the relay helix, is more than an order of magnitude faster than ATP hydrolysis. The relay helix undergoes this structural transition within a few milliseconds after ATP binding, with a rate in agreement with that of fluorescence changes of single tryptophan mutant at active site, previously attributed to ATP binding (26). These results show that ATP binding plays the crucial role in the recovery stroke, contradicting the classic model of myosin function, in which ATP hydrolysis is tightly coupled to the recovery stroke and serves as its driving force (reviewed in ref. 4). ATP hydrolysis is a relatively slow process, increasing the bent population  $(M^{**})$  of the relay helix only indirectly by mass action, converting  $M^{**}.T$  to  $M^{**}.D.P$  (step 3 in Scheme 2). The recovery stroke precedes ATP hydrolysis, which is needed not to fuel the recovery stroke but to facilitate product release and continue the cycle.

**Energy Landscape of Myosin Structural Transitions.** The temperature dependence of rate constants was interpreted according to transition state theory (27) assuming linear temperature dependence for thermodynamic parameters (an approximation for myosin in this temperature range). The free energy of activation for each step in Scheme 2, as well as the corresponding enthalpy and entropy of activation, were determined (Eq. 6 and Fig. 2). Starting from the collision complex  $M^*.T$ , the formation of transition state 2 (Fig. 2) during the recovery stroke (step 2 in Scheme 2) is almost purely enthalpic. Enthalpy remains high after the recovery stroke, but the high entropy of the  $M^{**}$ . T state keeps the net free energy increase small ( $\Delta G = 4$  kJ at 20 °C), permitting the coexistence of  $M^*$  and  $M^{**}$  structural states when ATP is bound. The length of the myosin step along the actin filament in muscle is L =11 nm (28, 29), generating force F = 3.4 pN (29), so energy E =22.5 kJ/mol is required for the power stroke. According to our kinetic data,  $\Delta G = 64$  kJ/mol is available in transition state 3 during ATP hydrolysis (Fig. 2).  $M^{**}.T$  is the state with maximum entropy in this process (steps 1-3, Scheme 2), reflecting high configurational disorder, and the subsequent transition state 3 has the lowest entropy and highest free energy. Thus a disorderto-order transition provides the driving force for the subsequent power stroke, which is consistent with a recently trapped acto-

Table 1. Rate constants (Scheme 2) determined from data in Fig. 1

	$T=4^{\circ}\text{C}$	$T=10^{\circ}\mathrm{C}$	$T=20^{\circ}\mathrm{C}$
k <sub>1</sub> , μM <sup>-1</sup> s <sup>-1</sup>	1.3 ± 0.5	2.4 ± 1.6	2.4 ± 1.7
$k_{-1}$ , s <sup>-1</sup>	$0.4 \pm 0.4$	$0.5 \pm 0.4$	$0.4 \pm 0.4$
$k_2$ , s <sup>-1</sup>	$36.8 \pm 1.3$	$64 \pm 7$	152 ± 28
$k_{-2}$ , s <sup>-1</sup>	260 ± 11	$347 \pm 40$	559 ± 111
$k_3$ , s <sup>-1</sup>	$7.1 \pm 0.5$	$7.4 \pm 0.6$	$9.9 \pm 0.7$
$k_{-3}$ , s <sup>-1</sup>	$5.0 \pm 0.6$	$6.4 \pm 0.5$	9.7 ± 0.5

Uncertainties are SD from 40-50 fits.

myosin intermediate (30), suggesting that a disorder-to-order transition is the first step in force generation (30–32).

## Discussion

Myosin Structural and Biochemical States Are Loosely Coupled. The coexistence of two structural states ( $M^*$  and  $M^{**}$ ) in a single biochemical state (the myosin-ATP complex), during the transient phase of the myosin ATPase reaction, confirms our previous findings with nucleotide analogs bound to myosin at equilibrium (11, 21), implying loose coupling between myosin structural and biochemical states. This conclusion is further supported by the considerable width of the detected distance distributions (Fig. 1E), indicating that myosin does not adopt a single rigid structure but samples a wide range of conformations around the average state. Indeed, it is likely that the true myosin-ATP interaction is best described with a nonlinear (branched) mechanism (5), as suggested by Scheme 3. Thus Scheme 2 represents the predominant, but not exclusive, pathway of the reaction. Some steps shown in Scheme 3 have a low probability of occurring if they are strictly defined as in the crystal structures. For example, in the  $M^*$  crystal structure, switch loop I and switch loop II of the active site do not appear to be in the proper position for catalysis of ATP hydrolysis (14, 16), suggesting that step 3' in Scheme 3 is not likely to occur. Indeed the present study, coupled with previous studies, indicates precisely that structural changes in the force-generating region (11, 21) and the actin-binding cleft (22) are not tightly coupled to ligand binding at the active site. Rather, each crystal structure represents a trapped structural state among the much larger repertoire available to each biochemical state in solution (4). Future studies must be designed to determine precisely the temporal relationships between structural changes in different regions of myosin. The versatile interplay between populations of different structural and biochemical states in myosin isoforms probably serves as a tool for fine-tuning myosin performance.

Energetics and Directionality of Myosin's Cycle. Myosin's ability to interconvert freely between different structures raises several questions. How does it avoid nonproductive ATP hydrolysis? What determines the directionality of myosin structural transitions? Thermodynamic analysis of the system shows that enthalpic and entropic contributions to the changes in Gibbs free energy  $(\Delta G)$  during structural transitions are almost perfectly balanced ( $\Delta G$  changes between  $M^*.T$ ,  $M^{**}.T$ , and  $M^{**}.D.P$  states are small), so structural transitions, corresponding to steps 2 and 3 in Scheme 2, may occur without significant free energy loss (Fig. 2). At the same time, no further transition was observed from the  $M^{**}.D.P$  state, indicating a high free energy barrier for step 4 (Fig. 2), which prevents a spontaneous and nonproductive  $M^{**} \rightarrow M^*$  transition. This high energy of the myosin transition state in the  $M^{**} \rightarrow M^*$  reaction implies that the power stroke is not a simple mirror image of the recovery stroke. Actin binding

$$\mathsf{M} + \mathsf{T} \overset{k_1}{\rightleftharpoons} \mathsf{M}^\star. \mathsf{T} \overset{k_2}{\rightleftharpoons} \mathsf{M}^{\star\star}. \mathsf{T} \overset{k_3}{\rightleftharpoons} \mathsf{M}^{\star\star}. \mathsf{D}. \mathsf{P} \overset{k_4}{\rightleftharpoons} \mathsf{M}^\star. \mathsf{D}. \mathsf{P} \overset{k_5}{\rightleftharpoons} \mathsf{M}^\star. \mathsf{D} + \mathsf{P} \overset{k_6}{\rightleftharpoons} \mathsf{M}. \mathsf{D} \overset{k_7}{\rightleftharpoons} \mathsf{M} + \mathsf{D}$$

Scheme 2. Revised ATPase kinetic scheme for myosin, allowing loose coupling between biochemical and structural states. Same definitions as in Scheme 1.

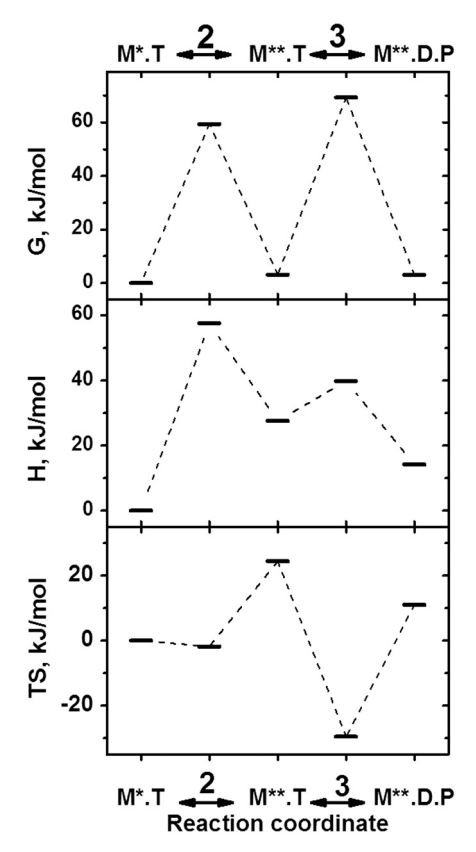


Fig. 2. Energy profiles at 20 °C for myosin structural changes during its interaction with ATP, determined from the structural kinetics reaction rates (Table 1). Myosin in transition state 2 (step 2 of Scheme 2) obtains energy from ATP binding,  $M^{**}.T$  is the state with maximum entropy, reflecting increased sampling of conformational space by myosin. Transition state 3 has maximum free energy, comparable to the energy required for the power stroke.

must lower the energy barrier, bringing directionality to the scheme. The present study is focused on structural changes in the force-generating region of myosin during the recovery stroke. A complete description of the myosin mechanism will require future studies on other phases of the myosin ATPase cycle (especially the power stroke, the force-generating reversal of the recovery stroke, induced by actin) and on other regions of the myosin motor, such as nucleotide and actin-binding sites of myosin.

In conclusion, in this work we introduce transient timeresolved FRET—a powerful tool that makes possible the direct analysis of structural kinetics. The key feature of (TR)<sup>2</sup>FRET is the resolution of protein structural states (Fig. 1E) with submillisecond time resolution (Fig. 1E). This technical advantage

		Biochemical state (bound ligand)				
		аро	Т	D.P	D	аро
ctural state	М	<b>M</b>	M.T ₹	⇒ M.D.P ⇒	. M.D ₹	<u>→ M</u>
	М*	M* <b>≥</b>	M*.T ₹	3' N*.D.P ₹	: M*.D <b>₹</b>	≥ M*
Struc	M**	<b>↑</b> Μ** <b>≥</b> ≥	M**.T =	3 4 <b>∜</b> <b>₹</b> M**.D.P <del>₹</del>	: M**D <b></b>	<sup>1↓</sup> ≥ M**

Scheme 3. Full scheme of myosin ATPase cycle. M, myosin; T, ATP; D, ADP; and P, inorganic phosphate. Structural states are populated differently in different biochemical states. States with clearly detected populations are shown in dark green. Light green shows required intermediate states. Green arrows show the most probable course of the reaction, with steps numbered as in Scheme 2. The biochemical state of myosin, determined by bound nucleotide, is loosely coupled to the structural state  $(M, M^*, \text{ and } M^{**})$ .

allowed us to monitor distinct structural states of the relay helix in the myosin molecular motor directly during the recovery stroke. The significance of this space-time resolution is threefold. First, our experiments directly resolved two structural states of myosin that were occupied in a single biochemical state, as determined by the bound nucleotide. Second, we were able to define not only the mean interprobe distance in each state but also the substantial disorder (presumably related to configurational entropy) present in each structural state. Finally, the mole fraction of each protein structural state was measured directly with millisecond resolution, leading to unambiguous determination of the kinetics and thermodynamics of the system, revealing how structural and biochemical changes are coupled. This study demonstrates the power of the (TR)<sup>2</sup>FRET technique, revealing real-time protein structural kinetics induced by protein-ligand interactions.

## **Materials and Methods**

Protein Preparation and Labeling. Mutants of Cys-lite Dictyostelium discoideum myosin motor domain were constructed, expressed, and purified as described previously (33). For FRET measurements, the protein (50  $\mu M$ ) was first incubated with donor (45  $\mu$ M IAEDANS, Invitrogen) for 12 h on ice, then protein was diluted to 25  $\mu M$  and incubated for 2 h on ice with 100-μM acceptor (DABCYL-C2-maleimide, Anaspec). After each labeling step, unreacted label was removed with size-exclusion spin columns (Pierce). Labeling buffer contained 20 mM MOPS (pH 7.5), 50 mM KCl, 6 mM MgCl<sub>2</sub>, and 1 mM EDTA. Complexes of myosin with nucleotide analogs were prepared as described previously (20).

ATPase Assays. Myosin ATPase activity was measured (T = 25 °C in 10 mM Tris, 6 mM MgCl<sub>2</sub>, 5 mM ATP, pH 7.5) in the presence and absence of actin, by the liberation of inorganic phosphate (34). The dependence of myosin ATPase activity on actin concentration was fitted to determine  $V_{max}$  (activity at saturating actin) as reported in Table 2. As reported previously (11), both basal and actin-activated ATPase activities were comparable (within a factor of 2) between unlabeled and labeled proteins and were also comparable (within a factor of 2) to values reported for other Dictyostelium myosin constructs (20, 22, 33), indicating that neither mutations nor labeling caused significant effects on myosin catalytic activity (Table 2).

(TR)<sup>2</sup>FRET Experiments. TR-FRET experiments were performed with an HPTRF instrument, utilizing direct waveform recording as described previously (11, 13). Fluorescence of IAEDANS-myosin was excited with the third harmonic (355 nm) of a passively Q-switched microchip yttrium aluminum garnet laser (NanoUV-355, JDS Uniphase), operated at a pulse repetition frequency of 10 kHz, and selected with a 420-nm long-pass glass filter. To avoid anisotropy effects, fluorescence was passed through a polarizer oriented at the magic angle. Fluorescence signals were detected after every laser pulse with a photomultiplier module (Hamamatsu H5773-20, rise time 0.78 ns) and acquired with a transient digitizer (Acgiris DC252) with time resolution of 0.125 ns (8 GS/s). The instrument response function (IRF) was acquired with scattered light at the same instrument settings as in the fluorescence measurement, except that there was no emission filter and the emission polarization was vertical. To obtain (TR)<sup>2</sup>FRET data, a stopped-flow apparatus (SFM-20. Bio-Logic) was attached to the fluorometer described above to measure transient kinetics of the myosin-ATP reaction. Myosin and ATP solutions were loaded into syringes, and the total flow rate through the mixer was 8 mL/s, giving a dead time of 1.4 ms. Donor fluorescence waveforms, consisting of 500 points (each having  $S/N \ge 100$ ) spaced 0.125 ns apart, were acquired after every laser pulse (10 kHz). All fluorescence experiments were performed in a buffer containing 20 mM 4-(2-hydroxyethyl)-1-piperazinepropanesulfonic acid, 6 mM MgCl<sub>2</sub>, 1 mM EGTA, pH 8.0.

Table 2. Effect of labeling on functional properties of Dictyostelium myosin

		D515C:K498C	A639C:K498C
$V_{\rm basal}$ , s <sup>-1</sup>	unlabeled	0.15	0.17
	labeled	0.08	0.10
$V_{\rm max}$ , s <sup>-1</sup>	unlabeled	3.8	4.4
	labeled	2.5	5.1

**Analysis of (TR)**<sup>2</sup>**FRET Data.** The observed donor-only waveform  $F_{Dobs}(t)$  was fitted by a simulation  $F_{Dsim}(t)$ , consisting of a multiexponential decay  $F_D(t)$  convolved with the IRF (from light scatter):

$$F_D(t) = \sum_{i=1}^n A_i \exp(-t/\tau_{Di}),$$

$$F_{D\text{sim}}(t) \int_{-\infty}^{+\infty} IRF(t-t')F_D(t')dt',$$
[1]

where  $\tau_{Di}$  are donor-only fluorescence lifetimes. We found that n=2 in Eq. 1 was sufficient, i.e., n=3 did not reduce the residual or  $\chi^2$ . The fluorescence signal of donor-acceptor labeled myosin,  $F_{\rm DA}(t)$ , was fitted by assuming that the only change in the donor fluorescence was increased rate of decay due to energy transfer:

$$F_{\mathrm{DA}}(t) = \int_{-\infty}^{+\infty} \rho(R) \cdot \sum_{i=1}^{n} A_i \exp\{(-t/\tau_{Di})(1 + [R_{0i}/R]^6)\} dR,$$
[2]

where  $A_i$  and  $\tau_{Di}$  were determined from the fit to Eq. 1, and the Förster distance  $R_{0i}$  was determined as described previously (11).

The probability distribution  $\rho(\mathbf{R})$ , a sum of Gaussian functions, accounts for flexibility:

$$\begin{split} \rho(R) &= \sum_{j=1}^m X_j \sigma_j^{-1} (2\pi)^{-1/2} \exp(-[(R-R_j)^2/(2\sigma_j^2)]), \\ \sigma_j &= \text{FWHM}_j/[2\times (2\ln 2)^{1/2}]. \end{split}$$
 [3]

After addition of ATP, the best fit was consistently obtained for m=2, corresponding to two structural states (11):  $M^*$  (prerecovery, straight relay helix), having mole fraction  $X^*$ , distance  $R^*$ , and width FWHM\*; and  $M^{**}$  (postrecovery, bent relay helix), having mole fraction  $X^{**}=1-X^*$ , distance  $R^{**}$ , and width FWHM\*\*. The observed waveform  $F_{D+Aobs}(t)$  was fitted by  $F_{D+Asim}(t)$ :

$$\begin{split} F_{D+A}(t) &= X_D F_D(t) + (1-X_D) F_{\mathrm{DA}}(t), \\ F_{D+A\mathrm{sim}}(t) &= \int_{-\infty}^{+\infty} \mathrm{IRF}(t-t') \cdot F_{D+A}(t') dt', \end{split} \tag{4}$$

where  $X_D$  is the fraction of donor-labeled proteins lacking acceptor.

Each set of fluorescence waveforms from a  $(TR)^2$ FRET experiment was fitted globally to Eq. **4**. Amplitudes  $A_i$ , lifetimes  $\tau_i$ , distances  $R^*$  and  $R^{**}$ , widths FWHM\* and FWHM\*\*, and the fraction of donor-only labeled myosin

- Chizhov I, et al. (1996) Spectrally silent transitions in the bacteriorhodopsin photocycle. Biophys J 71:2329–2345.
- Boehr DD, McElheny D, Dyson HJ, Wright PE (2006) The dynamic energy landscape of dihydrofolate reductase catalysis. Science 313:1638–1642.
- Henzler-Wildman K, Kern D (2007) Dynamic personalities of proteins. Nature 450:964–972.
- Thomas DD, Kast D, Korman VL (2009) Site-directed spectroscopic probes of actomyosin structural dynamics. Annu Rev Biophys 38:347–369.
- Malnasi-Csizmadia A, Kovacs M (2010) Emerging complex pathways of the actomyosin powerstroke. Trends Biochem Sci 35:684–690.
- Johnson KA, Taylor EW (1978) Intermediate states of subfragment 1 and actosubfragment 1 ATPase: Reevaluation of the mechanism. *Biochemistry* 17:3432–3442.
- Malnasi-Csizmadia A, Woolley RJ, Bagshaw CR (2000) Resolution of conformational states of *Dictyostelium* myosin II motor domain using tryptophan (W501) mutants: implications for the open-closed transition identified by crystallography. *Biochemistry* 39:16135–16146
- 8. Sun M, et al. (2006) Dynamics of the upper 50-kDa domain of myosin V examined with fluorescence resonance energy transfer. *J Biol Chem* 281:5711–5717.
- Sun M, Rose MB, Ananthanarayanan SK, Jacobs DJ, Yengo CM (2008) Characterization
  of the pre-force-generation state in the actomyosin cross-bridge cycle. Proc Natl Acad
  Sci USA 105:8631–8636.
- Xing J, Jayasundar JJ, Ouyang Y, Dong WJ (2009) Forster resonance energy transfer structural kinetic studies of cardiac thin filament deactivation. J Biol Chem 284:16432–16441.
- Agafonov RV, et al. (2009) Structural dynamics of the myosin relay helix by timeresolved EPR and FRET. Proc Natl Acad Sci USA 106:21625–21630.

 $X_D$  were linked and varied simultaneously for all waveforms during the global fit. Only  $X^{**}$  (the mole fraction of the  $M^{**}$  structural state) was allowed to vary independently for every waveform (every kinetic time point). The fraction  $X_D$  of donor-only labeled myosin mutant was allowed to vary between different protein preparations.

**Analysis of Recovery Stroke Kinetics.** To determine kinetic constants of the myosin–ATP reaction, the time-dependent trace of the  $M^{**}$  mole fraction [ $X^{**}$ , obtained by fitting the  $(TR)^2$ FRET data as described in Eqs. **2–4**] was fitted according to the solution of the system of differential equations for  $M^{**}$  (Eq. **5**):

$$\begin{split} d[M]/dt &= -k_1[M][T] + k_{-1}[M^*.T] \\ d[M^*.T]/dt &= k_1[M][T] - k_{-1}[M^*.T] - k_2[M^*.T] + k_{-2}[M^{**}.T] \\ d[M^{**}.T]/dt &= k_2[M^*.T] - k_{-2}[M^{**}.T] - k_3[M^{**}.T] \\ &+ k_{-3}[M^{**}.D.P] \\ d[M^{**}.D.P]/dt &= k_3[M^{**}.T] - k_{-3}[M^{**}.D.P] \end{split}$$

In Eq. 5, molecular species and rate constants are defined as in Scheme 2. Each equation describes the time evolution of each myosin state. Structural states are indicated by M,  $M^*$ , and  $M^{**}$ ; biochemical states are defined by the bound ligand (apo, T, D.P). Positive and negative terms describe the increase and decrease of structural state concentration due to forward and reverse transitions in Scheme 2. The time dependence of system was solved in Wolfram Mathematica 5.1 using the NDSolve routine. The fit to experimental data was realized with the NMinimize routine, using the Differential Evolution algorithm, with 10,000 initial parent points, scaling factor 1, and cross probability 0.8.

The temperature dependence of rate constants was analyzed in terms of transition state theory (27). The free energy of activation was determined from

$$\Delta G_a = -RT \ln(kh/[k_B T]) = \Delta H_a - T \Delta S_a,$$
 [6]

where h is Planck's constant,  $k_B$  is Boltzmann's constant, R is the gas constant, and T is the temperature. The enthalpy and entropy of activation,  $\Delta H_a$  and  $\Delta S_a$ , were obtained from the temperature dependence of  $\Delta G$  (Eq. 6).

**ACKNOWLEDGMENTS.** We thank Gregory Gillispie, Joseph Muretta, and David Kast for expert advice about the  $(TR)^2FRET$  instrumentation and methodology, and Octavian Cornea for assistance with preparation of the manuscript. This work was supported by National Institutes of Health Grants AR32961 (to D.D.T.), GM27906 (to D.D.T.), AG26160 (to D.D.T.), AR53562 (to Y.E.N.), AR59621 (to Y.E.N.), and a grant from the Minnesota Medical Foundation (YEN)

- Kast D, Espinoza-Fonseca LM, Yi C, Thomas DD (2010) Phosphorylation-induced structural changes in smooth muscle myosin regulatory light chain. Proc Natl Acad Sci USA 107:8207–8212.
- Muretta JM, et al. (2010) High-performance time-resolved fluorescence by direct waveform recording. Rev Sci Instrum 81:103101–103108.
- Fisher AJ, et al. (1995) X-ray structures of the myosin motor domain of *Dictyostelium discoideum* complexed with MgADP.BeFx and MgADP.AIF4. *Biochemistry* 34: 8960–8972.
- Houdusse A, Kalabokis VN, Himmel D, Szent-Gyorgyi AG, Cohen C (1999) Atomic structure of scallop myosin subfragment S1 complexed with MgADP: A novel conformation of the myosin head. Cell 97:459–470.
- Geeves MA, Holmes KC (1999) Structural mechanism of muscle contraction. Annu Rev Biochem 68:687–728.
- Malnasi-Csizmadia A, et al. (2001) Kinetic resolution of a conformational transition and the ATP hydrolysis step using relaxation methods with a Dictyostelium myosin Il mutant containing a single tryptophan residue. *Biochemistry* 40:12727–12737.
- Shriver JW, Sykes BD (1981) Phosphorus-31 nuclear magnetic resonance evidence for two conformations of myosin subfragment-1.nucleotide complexes. *Biochemistry* 20:2004–2012
- Naber N, Purcell TJ, Pate E, Cooke R (2007) Dynamics of the nucleotide pocket of myosin measured by spin-labeled nucleotides. Biophys J 92:172–184.
- Agafonov RV, Nesmelov YE, Titus MA, Thomas DD (2008) Muscle and nonmuscle myosins probed by a spin label at equivalent sites in the force-generating domain. Proc Natl Acad Sci USA 105:13397–13402.
- Nesmelov YE, Agafonov RV, Burr AR, Weber RT, Thomas DD (2008) Structure and dynamics of the force-generating domain of myosin probed by multifrequency electron paramagnetic resonance. *Biophys J* 95:247–256.

- 22. Klein JC, et al. (2008) Actin-binding cleft closure in myosin II probed by site-directed spin labeling and pulsed EPR. Proc Natl Acad Sci USA 105:12867-12872.
- 23. Shih WM, Gryczynski Z, Lakowicz JR, Spudich JA (2000) A FRET-based sensor reveals large ATP hydrolysis-induced conformational changes and three distinct states of the molecular motor myosin. Cell 102:683-694.
- 24. Trybus KM, Taylor EW (1982) Transient kinetics of adenosine 5'-diphosphate and adenosine 5'-(beta, gamma-imidotriphosphate) binding to subfragment 1 and actosubfragment 1. Biochemistry 21:1284–1294.
- 25. Gyimesi M, et al. (2008) The mechanism of the reverse recovery step, phosphate release, and actin activation of Dictyostelium myosin II. J Biol Chem 283:8153-8163.
- 26. Kovacs M, Malnasi-Csizmadia A, Woolley RJ, Bagshaw CR (2002) Analysis of nucleotide binding to Dictyostelium myosin II motor domains containing a single tryptophan near the active site. J Biol Chem 277:28459-28467.
- 27. Eyring H (1935) The activated complex in chemical reactions. J Chem Phys 3:107–115.
- 28. Finer JT, Simmons RM, Spudich JA (1994) Single myosin molecule mechanics: Piconewton forces and nanometre steps. Nature 368:113-119.

- 29. Higuchi H, Goldman YE (1995) Sliding distance per ATP molecule hydrolyzed by myosin heads during isotonic shortening of skinned muscle fibers. Biophys J 69:1491-1507.
- 30. Thompson AR, Naber N, Wilson C, Cooke R, Thomas DD (2008) Structural dynamics of the actomyosin complex probed by a bifunctional spin label that cross-links SH1 and SH2. Biophys J 95:5238-5246.
- 31. Thomas DD, Ramachandran S, Roopnarine O, Hayden DW, Ostap EM (1995) The mechanism of force generation in myosin: A disorder-to-order transition, coupled to internal structural changes. Biophys J 68:135S-141S.
- 32. Davis JS, Epstein ND (2009) Mechanistic role of movement and strain sensitivity in muscle contraction. Proc Natl Acad Sci USA 106:6140-6145.
- 33. Korman VL, Anderson SE, Prochniewicz E, Titus MA, Thomas DD (2006) Structural dynamics of the actin-myosin interface by site-directed spectroscopy. J Mol Biol 356:1107-1117.
- 34. Lanzetta PA, Alvarez LJ, Reinach PS, Candia OA (1979) An improved assay for nanomole amounts of inorganic phosphate. Anal Biochem 100:95-97.